Electrical Conductivity of Doped Organic Semiconductors Limited by Carrier-Carrier Interactions

Koopmans, Marten; Leiviskä, Miina A T; Liu, Jian; Dong, Jingjin; Qiu, Li; Hummelen, Jan C; Portale, Giuseppe; Heiber, Michael C; Koster, L Jan Anton

Published in:
ACS Applied Materials & Interfaces

DOI:
10.1021/acsami.0c15490

Publication date:
2020

ACS APPLIED MATERIALS & INTERFACES

www.acsami.org

Research Article

Electrical Conductivity of Doped Organic Semiconductors Limited by Carrier–Carrier Interactions

Marten Koopmans,[‖] Miina A. T. Leiviskä,[‖] Jian Liu, Jingjin Dong, Li Qiu, Jan C. Hummelen, Giuseppe Portale, Michael C. Heiber, and L. Jan Anton Koster*

Cite This: *ACS Appl. Mater. Interfaces* 2020, 12, 56222–56230

Read Online

ACCESS | Metrics & More | Article Recommendations | Supporting Information

ABSTRACT: High electrical conductivity is a prerequisite for improving the performance of organic semiconductors for various applications and can be achieved through molecular doping. However, often the conductivity is enhanced only up to a certain optimum doping concentration, beyond which it decreases significantly. We combine analytical work and Monte Carlo simulations to demonstrate that carrier–carrier interactions can cause this conductivity decrease and reduce the maximum conductivity by orders of magnitude, possibly in a broad range of materials. Using Monte Carlo simulations, we disentangle the effect of carrier–carrier interactions from carrier–dopant interactions. Coulomb potentials of ionized dopants are shown to decrease the conductivity, but barely influence the trend of conductivity versus doping concentration. We illustrate these findings using a doped fullerene derivative for which we can correctly estimate the carrier density at which the conductivity maximizes. We use grazing-incidence wide-angle X-ray scattering to show that the decrease of the conductivity cannot be explained by changes to the microstructure. We propose the reduction of carrier–carrier interactions as a strategy to unlock higher-conductivity organic semiconductors.

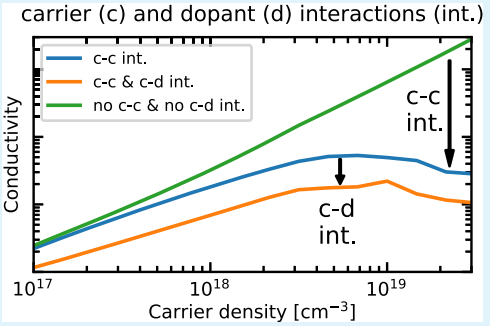

KEYWORDS: *organic semiconductors, doping, electrical conductivity, Coulomb interaction, kinetic Monte Carlo simulation, GIWAXS*

1. INTRODUCTION

Electrical conductivity is a key parameter in many organic electronic devices. In organic light-emitting diodes (OLEDs), organic solar cells (OSCs), and perovskite solar cells, increasing conductivity by doping can reduce ohmic losses,[1−3] and in thermoelectric generators, electrical conductivity is one of the key parameters.[4] Increasing the conductivity is most easily achieved by increasing the number of charge carriers by doping. Doping in organic semiconductors, however, is not a straightforward process as dopants need to react chemically with the host to yield free charges. The efficiency of this reaction varies, and therefore, the number of free charges per dopant molecule, or doping efficiency, also varies.[5]

Experimentally, it is observed that the electrical conductivity of a large number of organic semiconductors shows a maximum: first, the conductivity increases upon increasing doping density, but after the maximum the conductivity begins to decrease with increasing doping density. This behavior is observed in both polymer and small-molecule semiconductors doped with a wide variety of dopants[6−25] and can limit device performance in applications.[1−4] The carrier density at which the maximum in conductivity is observed ranges from 10^{18} to 10^{21} cm^{-3}.[6,14,18,20,22,26−29] The decrease in conductivity is often attributed to changes in the microstructure as a consequence of heavy doping. However, we have previously shown that even when using vapor doping, where there are no observable changes in the microstructure, the maximum in conductivity persists.[28]

Charge carrier transport in disordered organic semiconductors is usually described as a series of events where a charge carrier hops from one localized state to another.[30] The mobility of the charge carriers is proportional to the rate at which hopping events occur, which in turn is governed by the energetic and spatial distance of the hopping sites. The disordered nature of such disordered organic semiconductors manifests itself as a broad distribution of site energies and, when carrier density is low, a low intrinsic mobility of the charge carriers. Above a certain critical carrier concentration, the inherently low conductivity can be increased by introducing more carriers to the system, as this facilitates the filling of the low-energy trap sites.[31−34] However, charge carriers are introduced by doping, which also introduces oppositely charged dopant ions as the number of (free and bound) charge carriers equals the number of reacted dopants. The release of charge carriers is facilitated by the energetic

Received: August 28, 2020
Accepted: November 20, 2020
Published: December 2, 2020

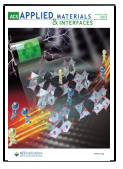

https://dx.doi.org/10.1021/acsami.0c15490
ACS Appl. Mater. Interfaces 2020, 12, 56222–56230

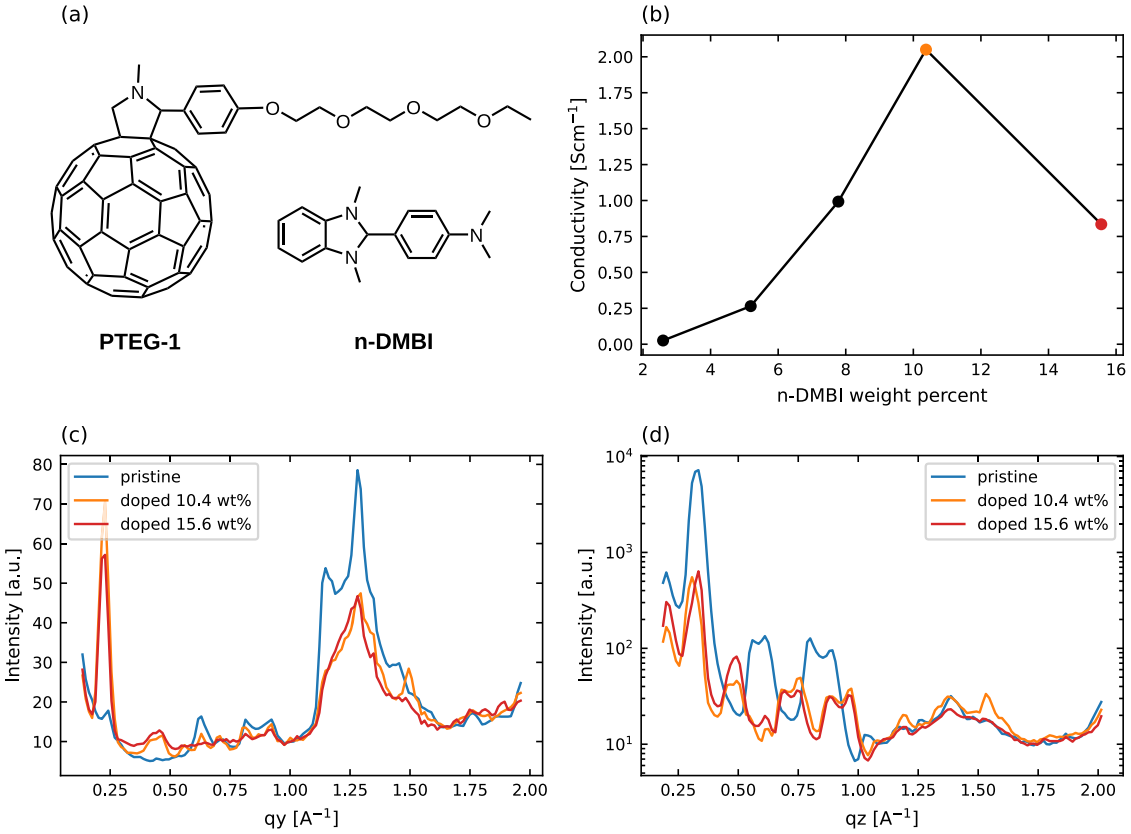

Figure 1. (a) Host, PTEG-1, and dopant, *n*-DMBI used in the other panels. (b) Conductivity of thin films of PTEG-1 doped with varying amounts of *n*-DMBI. (c, d) Line scans of GIWAXS measurements performed on PTEG-1 samples doped to varying weight percentages with *n*-DMBI.

disorder. However, the dopant Coulomb potentials trap most mobile charge carriers to nearest or next nearest-neighbor hopping sites.[35−37] The transport phenomena in doped disordered organic semiconductors are therefore typically explained on the basis of the interactions between dopant ions and mobile charge carriers.

Arkhipov et al.[38,39] introduced a model in which the Coulombic traps created by the dopant ions limit the charge carrier mobility at low-to-moderate doping concentrations while at high doping concentrations the overlap of the traps smoothens the potential landscape and increases the mobility.[38,39] This was experimentally confirmed for a large number of doped organic systems where the conductivity at low doping density appears to be limited by carrier−dopant interactions, while at higher dopant loading, the dependence of conductivity on carrier−dopant interactions diminishes.[40] The low-energy tail of density-of-states was proposed to broaden due to the increased energetic disorder induced by the dopant ions. The behavior predicted by the Arkhipov model is observed in a number of kinetic Monte Carlo (KMC) simulations[35,41] and it appears to be applicable for low to moderate doping densities. The experimentally observed conductivity maximum, however, would contradict this model: increasing the doping density would lead to an increasingly smooth potential landscape resulting in an upward trend in conductivity.[38,39] This indicates it is unlikely that dopant−carrier (d−c) interaction−s could cause this maximum in conductivity.

While dopant−carrier interactions are indeed recognized as an important factor, the effect of carrier−carrier (c−c) interactions has received less attention. This is mainly because their repulsive interaction introduces no traps or barriers that could reduce charge carrier mobility[38] or because the carrier density is negligibly small.[41] Contrary to these findings, Liu et al. have shown using kinetic Monte Carlo (KMC) simulations that carrier−carrier interactions in pristine, undoped organic semiconductors can limit the mobility at carrier densities above 10^{18} cm^{-3}.[42] Moreover, in disordered inorganic semiconductors carrier−carrier interactions result in the development of a soft gap in the density-of-states at the Fermi level.[43,44] This is a result of the requirement that for a system in ground state any electron transfer must increase the energy of the system. This so-called Coulomb gap was first derived by Efros and Shklovskii (ES)[43] and can act as a fingerprint for the relevance of carrier−carrier interactions.

Until now, it remains unclear what governs the transport in highly doped disordered organic semiconductors. At a high carrier density, the charge carrier mobility could increase because of overlapping dopant potentials,[38,39] or it could decrease because of carrier−carrier interactions.[42] It is therefore important to consider both dopant−carrier and carrier−carrier interactions to establish a complete description of the charge transport process in highly doped organic semiconductors.

Here, we address and elucidate the effect of morphology, dopant−carrier interactions, and carrier−carrier interactions on the conductivity of doped organic semiconductors. We first discuss the occurrence of a maximum in conductivity in doped organic semiconductors based on the literature and our previous work. To assess the role of morphology, we use grazing-incidence wide-angle X-ray scattering (GIWAXS) on a doped fullerene derivative and find that it cannot explain the

https://dx.doi.org/10.1021/acsami.0c15490
ACS Appl. Mater. Interfaces 2020, 12, 56222−56230

decrease in conductivity at high doping. We then use ES theory on carrier−carrier interactions to predict the carrier density at which the maximum of conductivity occurs. Finally, we show KMC simulations exhibiting a maximum in conductivity at a charge carrier density that corresponds to that observed experimentally. The maximum is observed both in the presence and absence of dopants. Overall, we show that carrier−carrier interactions lower the conductivity by orders of magnitude at high doping densities and therefore propose the suppression of carrier−carrier interactions as a key strategy for creating higher-conductivity organic semiconductors.

2. RESULTS

It has been observed in many different host and dopant combinations that the conductivity maximizes and then decreases with increasing doping concentration.[6−25] This decrease at high doping concentrations is often attributed to changes in morphology.[24,45] We previously conducted conductivity measurements on thin films of the fullerene derivative PTEG-1 doped with molecular dopant n-DMBI (see Figure 1a for their structure). Figure 1b shows the conductivity for varying molar doping concentration of PTEG-1 doped with *n*-DMBI as reported.[18] As the fraction of dopant in the system was increased the conductivity increased, peaked, and then decreased at high doping concentrations.

To check whether changes to the morphology are a likely cause of the conductivity decrease at high doping densities we performed GIWAXS measurements on three PTEG-1 samples with different doping concentrations of *n*-DMBI. The measurements were performed on a pristine PTEG-1 sample, a 10 wt % doped sample, and a 15 wt % doped sample. These densities were chosen because previous measurements in Figure 1b have shown that 10 wt % doping yields the maximum conductivity, while at 15 wt % doping, the conductivity starts to decrease. If the maximum in conductivity is caused by a deteriorating microstructure upon adding too many dopants, there should be significant microstructural differences between the two doped samples.

Figure 1c,d shows that at least for PTEG-1 doped with *n*-DMBI, this is unlikely to be the case. The morphology changed upon doping the pristine PTEG-1 system, but the morphology for 15% doping concentration was very similar to that of the 10% doping concentration sample. This means that although there are microstructural changes in the film upon doping, the changes between different doping levels are small and cannot explain the decrease in conductivity for these samples. This indicates that in this system a different mechanism is likely causing the decrease in conductivity at high doping density. Having shown that morphology is unlikely to cause the conductivity maximum in our system, we look at dopant−carrier interactions and the less discussed carrier−carrier interactions as alternative possible explanations for the conductivity maximum.

We first address the carrier−carrier interactions analytically answering the question: at which doping density can we expect to see the effects of carrier−carrier interactions? Charge transport in an intrinsic organic semiconductor is often described as a series of hopping events between localized states that follow a Gaussian distribution in energy with a standard deviation σ of 75−100 meV.[30,46,47] The density of states (DOS) in the absence of Coulomb interactions is given by[30]

$$g_0(\epsilon) = \frac{1}{a^3\sqrt{2\pi\sigma^2}} \exp\left(-\frac{\epsilon}{2\sigma^2}\right) \quad (1)$$

where a is the lattice spacing. To provide an estimate for the onset of carrier−carrier interactions, we turn to the ES theory of the Coulomb gap. The width Δ of the Coulomb gap is given by[48]

$$\Delta = \frac{q^3\sqrt{g_0^F}}{(4\pi\kappa\varepsilon_0)^{3/2}} \quad (2)$$

where g_0^F is the DOS at the Fermi level in the absence of Coulomb carrier−carrier interactions, κ is the relative dielectric constant, ε_0 is the vacuum permittivity, and q is the unit charge. The problem is then reduced to finding g_0^F such that Δ is equal to the relevant energy scale. As the doping level increases, the Fermi level shifts and g_0^F will increase and so will the Coulomb gap energy Δ. In disordered organic semiconductors, the two relevant energies are the thermal energy k_BT and the energetic disorder of the DOS, σ. If the predicted Coulomb gap is of the order of the thermal energy k_BT or larger, then we expect Coulomb carrier−carrier interactions to start to affect the conductivity. We expect carrier−carrier interactions to dominate when Δ becomes larger than the energetic disorder in the system. Assuming a relative dielectric constant κ = 4, eqs 2 and 1 imply that carrier−carrier interactions will become notable ($\Delta = k_BT$) at a carrier density $n_c \approx 2 \times 10^{18}$ cm^{-3}. Carrier−carrier interactions will dominate ($\Delta = \sigma$) and likely limit the electrical conductivity at a carrier density of 1×10^{19} cm^{-3}. In the next section, we will compare these predicted critical carrier densities with KMC simulations.

Now that we have analytically shown that carrier−carrier interactions are expected to affect disordered organic semiconductors with localized charge carriers, we can investigate conductivity in these systems using KMC simulations. Using KMC simulations the effects of carrier−carrier interactions and dopant−carrier interactions can be disentangled. The effects of dopant counterions resulting from dopant−carrier (d−c) interactions and carrier−carrier (c−c) interactions are investigated by selectively turning them on and off in the simulations. We treat three cases: (1) no c−c and no d−c interactions, (2) c−c but no d−c interactions, (3) and c−c and d−c interactions. The resulting conductivity is investigated alongside with the DOS.

In KMC simulations, it is notoriously hard to get rid of the dependence of simulated trends on simulation parameters such as number of simulated hops or the simulated box size. In Figure S4, we show that if not enough hops are simulated in the KMC simulations, the trend can change drastically compared to the properly equilibrated result. The way we check for equilibrium is by checking the temperature of the charge carriers. When a simulation is initialized, the charge carriers start on sites that are the lowest in energy without accounting for carrier−carrier interactions. This means the carriers are in an excited configuration once we introduce carrier−carrier interactions and we need to let the charge carriers hop until they reach equilibrium, otherwise we risk overestimating the conductivity. We confirmed equilibration by fitting the occupied DOS (o-DOS) to the DOS times the Fermi−Dirac function. When the temperature of the charge carriers is higher than that of the lattice, equilibrium has not yet been reached, but when the resulting temperature is within 15% of our settings, we consider the simulation equilibrated.

https://dx.doi.org/10.1021/acsami.0c15490
ACS Appl. Mater. Interfaces 2020, 12, 56222−56230

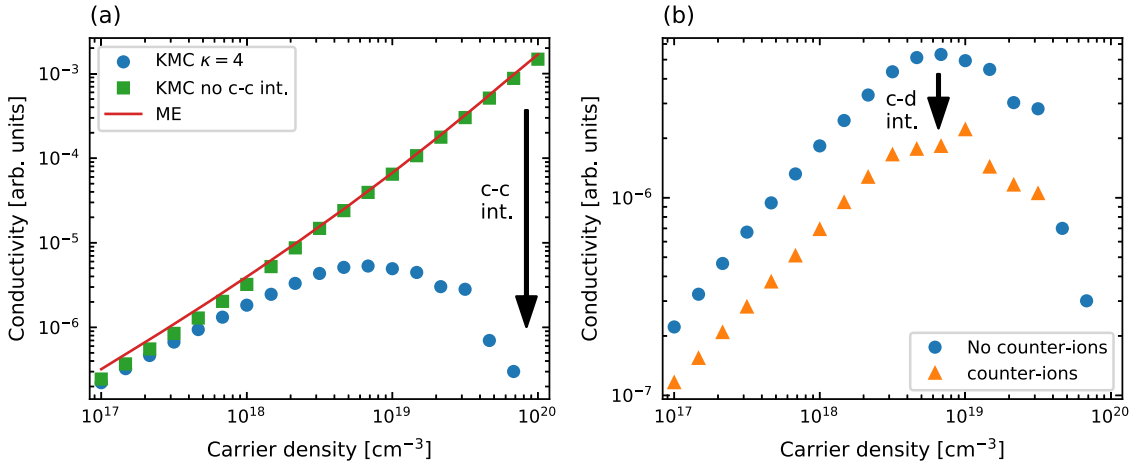

Figure 2. (a) KMC and ME simulations without counterions using the same parameters. KMC simulations (circles) at dielectric constants of 4 and at an arbitrarily large dielectric constant (squares) to eliminate carrier−carrier interactions. A dielectric constant of 1000 was used for this purpose. The arrow indicates the effect of carrier−carrier interactions, which become stronger as the carrier density increases. Master equation simulations (line) with the same input parameters as the KMC simulations are also shown. (b) KMC simulations with (triangles) and without (circles) Coulomb potentials of ionized dopants in equal number as free charge carriers.

Because of the difficulty reaching an equilibrated state, we also validate the KMC simulations against both SE theory on electron−electron interactions from the previous section and master equation (ME) simulations. Although the ME method does not include c−c or d−c interactions, at low charge carrier density the effect of c−c interactions is negligible compared to the effect of the intrinsic disorder. Therefore two of the three sets of KMC simulations can be at least partly validated using ME simulations.

Figure 2 shows the conductivity as a function of carrier density obtained from the KMC simulations and the ME simulations. Figure 2a shows that the effect of carrier−carrier interactions is very strong: at a carrier density of 10^{19} cm^{-3} carrier−carrier interactions reduce the conductivity by roughly 1 order of magnitude, while increasing the carrier density to 10^{20} cm^{-3} results in a conductivity reduction by 3 orders of magnitude. In Figure 2b, dopant counterion potentials are added to the simulations. We see that although the simulations that include dopant counterions show lower conductivity, as expected from the Arkhipov model, the trend is the same and the maximum in conductivity remains at the same charge carrier density of ∼10^{19} cm^{-3}. This shows that carrier−carrier interactions can cause the conductivity to peak at experimentally relevant doping densities in doped organic semiconductors. As indicated by the arrows in Figure 2, c−d interactions effectively shift the carrier density versus conductivity curve down to lower conductivity, meaning their effect is not strongly dependent on charge carrier density. The effect of c−c interactions only appears at higher densities, but dominates the high charge carrier density conductivity behavior.

The DOS of the simulations without counterions are collated in Figure 3 to better show the difference between the DOS at different charge carrier densities. It can be readily seen that the DOS becomes wider with increasing charge carrier density. Also, a shoulder appears at the lower-energy side of the DOS and becomes prominent at a carrier density of around 2.2 × 10^{18} cm^{-3}. It should be noted that this shoulder is purely a manifestation of carrier−carrier interaction as there are no counterions present in this simulation. Running the same simulation with dopant counterions yields roughly the same result as can be seen in Figure S2. When the charge carrier density reaches 10^{19} cm^{-3} a local minimum, i.e., Coulomb pseudogap, in the DOS can be observed. This pseudogap appears regardless of the presence of ionized dopants (see Figure S1).

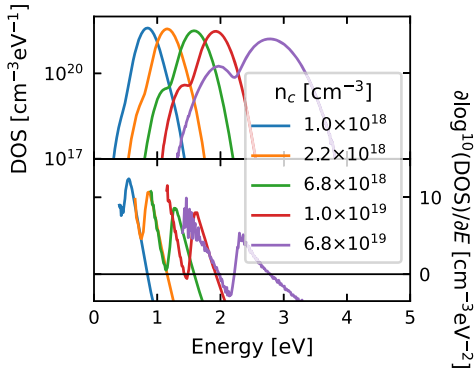

Figure 3. (Top) DOS as calculated using KMC simulations for increasing charge carrier densities (from left to right) in the absence of counterions. Increasing carrier density changes the shape of the DOS from a single Gaussian to an apparent superposition of two Gaussians. (Bottom) First derivative of the DOS with respect to energy, showing the first appearance of a valley in the DOS between 6.8 × 10^{18} and 1.0 × 10^{19} cm^{-3}.

Finally, we investigate the role of dopants in more detail. In the KMC simulations, a dopant is placed on a lattice point, but the Coulomb potential of the ionized dopant is calculated with an effective dopant radius added (r_{dop}) to the lattice distance. The r_{dop} determines the maximum Coulomb interaction strength possible between a mobile charge carrier and a dopant as the minimal possible distance between them is the r_{dop}. In Figure 2b, an effective dopant radius of 1 nm was used. When the effective dopant radius is 1 nm the maximum interaction energy is 0.36 eV. This value is chosen as it does not exceed the exciton binding energy of ∼0.4 eV.[49] A stronger interaction would render the charge carrier effectively bound. The impact of the r_{dop} on the electrical conductivity is shown in Figure 4, illustrating that the dopant ions do affect the conductivity depending on the r_{dop}. However, the impact of

https://dx.doi.org/10.1021/acsami.0c15490
ACS Appl. Mater. Interfaces 2020, 12, 56222−56230

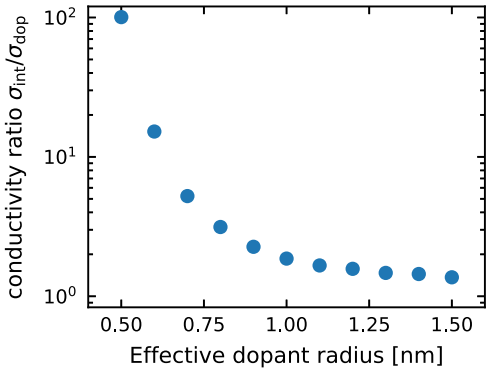

Figure 4. At a carrier density of 10^{17} cm^{-3}, the conductivity ratio between simulations without dopant potentials (σ_{int}) and simulations with dopant potentials (σ_{dop}).

carrier−carrier interactions at high charge carrier density (see Figure 2a) appears to be larger than that of the dopants even if a low r_{dop} is assumed.

3. DISCUSSION

We find a conductivity maximum using KMC simulations that include carrier−carrier and carrier−dopant interactions (see Figure 2). We find that the maximum conductivity is obtained at the same charge carrier density as in previous experimental conductivity measurements for PTEG-1 doped with *n*-DMBI (see Figure 1b). Our new experimental evidence (Figure 1c,d) suggests that there are no significant microstructural changes upon doping while the KMC simulations reproduce the maximum without accounting for morphology. This leads us to a conclusion that morphology changes are an unlikely explanation for the conductivity maximum in our experiments. We also observe that the Coulomb potentials of the ionized dopants are not the cause for the maximum in conductivity (Figure 2) as the maximum is present in the conductivity regardless of whether the dopant ions are implemented or not. This means we can exclude both typical explanations, i.e., morphology and dopants, for the maximum in conductivity.

A remaining explanation for the conductivity maximum is the carrier−carrier interactions. Experimentally, the maximum in conductivity is observed in various systems and the corresponding carrier density ranges from the order of 10^{18} to 10^{21} cm^{-3}.[6,14,18,20,22,26−29] Our analytical results using eq 2 that include both mobile charge carriers and dopants predict that carrier−carrier interactions start to dominate when the Coulomb gap width is larger than the energetic disorder, which occurs at a carrier density in the order of 10^{19} cm^{-3}. These effects are fundamental to the interaction of charge carriers and are as generally applicable as the effect of Coulomb attraction between dopant and mobile charge carriers. Our KMC simulations show that even in the absence of dopant ions a maximum in conductivity is observed at the same carrier density of 10^{19} cm^{-3}. Based on the combination of methods used here, we propose that the conductivity maximum is primarily a result of the carrier−carrier interactions. Considering the wide applicability of the analytical work and the range of different materials that could be simulated using similar KMC simulation settings, this is likely to be the case in many different disordered organic materials.

It should be noted that the carrier density at which the conductivity maximum occurs is influenced by the dielectric constant as can be seen in eq 2. When the dielectric constant increases, the charges are more screened and therefore their interaction will be weaker. As a result, the conductivity maximum is expected to shift to higher charge carrier densities. The dielectric constants of disordered organic semiconductors vary considerably. For example, the dielectric constant of PTEG-1 is 5.7 while that of conjugated polymers is typically lower.[50] In our KMC simulations we choose a relative dielectric constant of 4. A second factor affecting the interaction of charge carriers is their localization. Both the analytical work and the KMC simulations assume highly localized charges, but in many molecular semiconductors, charge carriers can be quite delocalized. This can therefore provide an explanation for why in some polymers the carrier density at the maximum conductivity is higher[6,22,29] than that calculated in the KMC simulations (Figure 2). Improved screening of charges and increased delocalization of charge carriers both could serve as strategies to reduce unwanted carrier−carrier interaction.

The negative effect of the carrier−carrier interactions on the conductivity can be linked to the development of a Coulomb pseudogap, which forms at high carrier densities regardless of the presence or absence of dopant counterions (Figure 3). This indicates that this feature is a sole consequence of the carrier−carrier Coulomb interactions rather than a result of the dopant ions. At high carrier densities, this soft gap forms at the Fermi level as seen in Figure 3 and, as a consequence, reduces the number of available hopping sites in the vicinity of the Fermi level. This means that the carriers are forced to hop to higher-energy sites, which again reduces the rate of hopping as given by the Miller−Abrahams expression.[51] Such a modification of the DOS upon doping has been previously reported experimentally,[35] but the development of the low-energy shoulder was attributed to the impact of the dopant ions as described by Arkhipov.[39] However, we have observed that the broadening of DOS as a result of the dopant−dopant interactions in Figure S1 and as a result of carrier−carrier interactions in Figure 3 is different from the DOS broadening as a result of carrier−dopant interactions, as described in the Arkhipov model. Moreover, when the mobile charge carriers and dopants are included, the DOS is a superposition of two Gaussians rather than a Gaussian with an exponential tail, as expected by the Arkhipov model.

The reliability of the KMC simulations can be validated by considering that at low carrier density the ME and KMC simulations agree quantitatively (Figure 2a). Moreover, the experimentally, analytically and numerically obtained critical carrier densities at which the conductivity reaches a maximum match very well. Also, the density of ∼10^{18} cm^{-3} at which the Coulomb pseudogap width equals k_BT and is predicted to start influencing conductivity coincides with the carrier density found by Liu et al.[42]

In conclusion, we have shown that while the Coulomb potentials of the ionized dopants are not the cause for the maximum in conductivity, they still have a significant role in governing the conductivity of the system. As seen in Figure 2b, the dopant ions lower the overall conductivity, meaning that attempts to shield the dopant potentials might advance the quest for higher-conductivity materials. This observation is in agreement with experimental work where dopant ions were shielded by increasing the dopant radius.[6] However, the maximum achievable increase in conductivity upon removing the dopant ions from the system was limited to less than an order of magnitude when we assumed the depth of the

https://dx.doi.org/10.1021/acsami.0c15490
ACS Appl. Mater. Interfaces 2020, 12, 56222−56230

Coulomb potential to be limited to the exciton binding energy. In contrast, decreasing the Coulomb interaction between mobile charge carriers (Figure 2a) resulted in conductivity increase by more than 3 orders of magnitude. Considering this, reducing carrier−carrier interactions through reduced carrier localization or increased screening of charges could be the more effective one to design higher-conductivity materials.

4. CONCLUSIONS

We show using both Efros−Shklovskii theory and kinetic Monte Carlo simulations that a Coulomb pseudogap appears in the density of states at a charge carrier density of $\sim 10^{19}$ cm^{-3}. This coincides with the charge carrier density at which the maximum conductivity was previously reported for the fullerene derivative PTEG-1 doped to varying degrees with molecular dopant *n*-DMBI. This Coulomb pseudogap is a manifestation of carrier−carrier interactions and limits the conductivity regardless of the presence of dopant Coulomb potentials. We performed GIWAXS measurements on the doped PTEG-1 samples to show that the microstructure does not change significantly from the optimally doped samples to over-doped samples, where the conductivity is lower due to an excess of dopants as reported previously.

Due to the broad applicability of the analytical work and the KMC simulations, we expect carrier−carrier interactions to play an important role in a wide range of both n-type and p-type disordered organic semiconductors at charge carrier densities of $\sim 10^{19}$ cm^{-3} and above. We show that at high dopant loading eliminating carrier−carrier interactions can increase the conductivity by orders of magnitude, while reducing carrier−dopant interactions leads to a much smaller gain in conductivity. This means that reducing carrier−carrier interactions could be a key strategy to find higher-conductivity organic semiconductors.

5. METHODS

5.1. Numerical Techniques. We used Excimontec v1.0.0-rc.3,[52] an open-source KMC simulation tool to simulate the hopping process in disordered organic semiconductors. The system was represented by a regular cubic grid with a lattice parameter, *a*, of 1 nm containing a fixed amount of charge carriers at high carrier density, where the lattice points are hopping sites for charge carriers. The number of charge carriers is set at ∼10 000 and the grid size was scaled to set the desired charge carrier density. For low charge carrier density, the grid dimensions were limited to 150 × 150 × 150 for memory saving purposes and because the grid size has no influence on the calculated physical properties of the system at these low carrier densities. Periodic boundary conditions in three dimensions were assumed to counteract finite size effects in the simulations. Simulations were performed both on systems containing only mobile charge carriers and on systems containing mobile charge carriers and immobile charged dopant ions, making the second system electrically neutral.

In the KMC simulations, a dopant was placed on a lattice point, but the Coulomb potential of the ionized dopant was calculated with r_{dop} added to the lattice distance. This means that the site energy was calculated as

$$E_{site} = E_{int} + \sum_{0}^{N_{dop}} V_C(r_{lat} + r_{dop}) \tag{3}$$

where E_{int} is the contribution from the intrinsic Gaussian disorder of the organic semiconductor, N_{dop} is the number of dopants, r_{lat} is the distance on the lattice from the site to the dopant, r_{dop} is the effective dopant radius, and V_C is the Coulomb potential of a single dopant at distance *r* given by

$$V_C(r) = \begin{cases} -\dfrac{q}{4\pi\varepsilon\kappa r}, & \text{if } r - r_{dop} < r_{cut} \\ 0, & \text{otherwise} \end{cases}$$

where r_{cut} is the cutoff radius, which we take to be one-tenth of the simulation volume length and therefore ∼2.2 times the cubic nearest-neighbor distance of the mobile charge carriers.

Both mobile charge carriers and dopants, if applicable, were initially placed at random lattice positions. The mobile charge carriers were then redistributed according to a rejection-free KMC algorithm until steady state was reached. For the hop rates in the KMC algorithm, a Miller−Abrahams expression was used[51] and a temperature of 300 K and an inverse localization length of 10 nm^{-1} was used to calculate the hopping rates. The hop rates therefore only depend on the distance and energy difference between an initial and target site. The site energies of lattice sites contain a static component from intrinsic disorder, which we took to be 77.6 meV, typical for a fullerene system, combined with the Coulomb potential of the dopant ions. Additionally, a dynamic component from the Coulomb interactions with mobile charge carriers surrounding the lattice site for which a dielectric constant of 4 was used.

For both static and dynamic Coulomb interactions an identical cutoff radius of 1/10 of the simulation volume length was used. Because of the scaling of the simulation volume this means that for the higher-density simulations, the cutoff radii were ∼2.2 times the cubic nearest-neighbor distance of the charge carriers. It has been shown that the average carrier separation roughly determines how large the Coulomb and cutoff radius should be.[53]

Different ways of defining the Coulomb potential of the ionized dopants were attempted, but the details did not change the outcome of the simulations. Upon completion of a hop, a selective recalculation procedure was used to calculate hopping rates for carriers near the initial and target sites up to a radius that equals the cutoff radius for the Coulomb interactions.

The simulation procedure then entailed putting the desired amount of mobile charge carriers and dopant ions in the simulation volume at random. An electric field of 10^7 V m^{-1} was then applied along a lattice direction of the simulation volume. Mobile charge carriers then hopped according to the described KMC algorithm for a certain number of hops to let the system cool down. After cooling, the simulation was continued until the statistical error on the output parameters was acceptable. To check the temperature of the simulation after the cooling period the o-DOS of the charge carrier was fit to the DOS times the Fermi−Dirac distribution. If the temperature of the fit Fermi−Dirac distribution is within 15% of the target temperature, we accept the simulation. If the temperature is too high we continue calculation until the desired temperature is reached. During the simulation period, the occupied density of states (o-DOS) is sampled once every 1000 hops and the density of states (DOS) is sampled once at the end of the simulation.

Doing KMC simulations on large enough simulation volumes with carrier−carrier interactions takes a huge computational effort. On the Peregrine computer cluster we used 1140 cores for roughly 20 days to get the data for Figure 2b. The statistical error was lower than expected meaning that the core count can be lowered slightly, but efforts to reduce the computation time might lead to systematic errors.

Master equation (ME) simulations were used for validating KMC simulation results. In this Gaussian disorder model (GDM) an uncorrelated Gaussian distribution of hopping sites was assumed to constitute the DOS. The GDM was used to calculate the dependence of conductivity on charge carrier density in the absence of Coulomb interactions. A simple cubic lattice was used as a grid for these simulations, where *a* is, as in the KMC simulations, 1 nm. To calculate the charge carrier mobility occupational probabilities of the lattice sites were used instead of physical charge carriers. At the start of the ME simulation, every site was assigned a random energy from a Gaussian distribution with a width of 77.6 meV. An electric field was applied along a lattice direction effectively tilting the energetic

https://dx.doi.org/10.1021/acsami.0c15490
ACS Appl. Mater. Interfaces 2020, 12, 56222−56230

landscape. The effect of this electric field was then calculated by solving the steady-state Pauli master equation for all target sites j

$$\sum_j [W_{i\to j} n_i(1 - n_j) - W_{j\to i} n_j(1 - n_i)] = 0 \quad (4)$$

where i is the initial site, $W_{i\to j}$ is the transition rate from i to j, $W_{j\to i}$ is the rate of the reverse transition, and n_i and n_j are the occupational probabilities of site i and j, respectively. For the transition rates $W_{i\to j}$ and $W_{j\to i}$, Miller−Abrahams hopping rates[51] were used with the same parameters as in the KMC simulations. The mobility was then calculated as

$$\mu = \frac{\sum_{ij} w_{i\to j} n_i(1 - n_j)(\vec{r_j} - \vec{r_i})\cdot\hat{F}}{n_c|\vec{F}|} \quad (5)$$

where $\hat{F} = \vec{F}/|\vec{F}|$ is the unit vector in the direction of the electric field, $\vec{F}$ is the electric field vector, $\vec{r_j}$ and $\vec{r_i}$ are the position vectors of the target and initial site of a hop with respect to some point, respectively, and n_c is the charge carrier density per unit volume.

5.2. Experimental Methods. *n*-DMBI was supplied by Sigma-Aldrich, and a previously reported procedure was used to synthesize PTEG-1.[50] Borosilicate glass substrates were washed using, in order of use, detergent, acetone, and isopropanol. Afterward, the substrates were dried with a nitrogen gun and received a UV−ozone treatment for 20 min. Various amounts of *n*-DMBI solution (5 mg mL^{-1} in chloroform) were mixed with a PTEG-1 solution (5 mg mL^{-1} in chloroform) to fabricate doped PTEG-1 films. The film thickness (d) was measured using ellipsometry to be between 40 and 50 nm. To measure electrical conductivity, a geometry using parallel line-shape Au electrodes with a width (w) of 13 mm and a channel length (L) of 100−300 μm as top contact was employed. In a N_2 glovebox, voltage-sourced two-point conductivity measurements were conducted. The electrical conductivity (σ) was calculated as $\sigma = (J/V \times L/(w \times d))$. For a reference measurement of commercial poly(3,4-ethylenedioxythiophene):poly(styrene sulfonate) (PEDOT:PSS) (Clevios P VP Al 4083) the conductivity was measured to be 0.06 S m^{-1}, well in line with the expected value between 0.02 and 0.2 S m^{-1}.

Grazing-incidence wide-angle X-ray scattering (GIWAXS) measurements were performed using a MINA X-ray scattering instrument built on a Cu rotating anode source (λ = 1.5413 Å). Two-dimensional (2D) patterns were collected using a Vantec500 detector (1024 × 1024 pixel array with pixel size 136 × 136 μm^2) located 93 mm away from the sample. The PTEG-1 films were placed in reflection geometry at certain incident angles α_i with respect to the direct beam using a Huber goniometer. GIWAXS patterns were acquired using incident angles from of 0.14°. The direct beam center position on the detector and the sample-to-detector distance were calibrated using the diffraction rings from standard silver behenate and Al_2O_3 powders. All of the necessary corrections for the GIWAXS geometry were applied to the raw patterns using the GIXGUI Matlab toolbox. The reshaped GIWAXS patterns, taking into account the inaccessible part in reciprocal space (wedge-shaped corrected patterns), are presented as a function of the vertical and parallel scattering vectors q_z and q_r, respectively. The scattering vector coordinates for the GIWAXS geometry are given by

$$q_x = \frac{2\pi}{\lambda}(\cos(2\theta_f)\cos(\alpha_f) - \cos(\alpha_i)) \quad (6)$$

$$q_y = \frac{2\pi}{\lambda}(\sin(2\theta_f)\cos(\alpha_f)) \quad (7)$$

$$q_z = \frac{2\pi}{\lambda}(\sin(\alpha_i) + \sin(\alpha_f)) \quad (8)$$

where $2\theta_f$ is the scattering angle in the horizontal direction and α_f is the exit angle in the vertical direction. The parallel component of the scattering vector is thus calculated as $q_r = \sqrt{q_x^2 + q_y^2}$.

■ ASSOCIATED CONTENT

Supporting Information

The Supporting Information is available free of charge at https://pubs.acs.org/doi/10.1021/acsami.0c15490.

DOS for intrinsic disorder, upon adding dopants, and upon adding mobile charge carriers; DOS for different densities of dopants; DOS at the Fermi level; and the effect of thermalization on the DOS (PDF)

■ AUTHOR INFORMATION

Corresponding Author

L. Jan Anton Koster − *Zernike Institute for Advanced Materials, University of Groningen, Groningen 9747 AG, The Netherlands;* orcid.org/0000-0002-6558-5295; Email: l.j.a.koster@rug.nl

Authors

Marten Koopmans − *Zernike Institute for Advanced Materials, University of Groningen, Groningen 9747 AG, The Netherlands;* orcid.org/0000-0002-2328-155X

Miina A. T. Leiviskä − *Zernike Institute for Advanced Materials, University of Groningen, Groningen 9747 AG, The Netherlands*

Jian Liu − *Zernike Institute for Advanced Materials, University of Groningen, Groningen 9747 AG, The Netherlands;* orcid.org/0000-0002-6704-3895

Jingjin Dong − *Zernike Institute for Advanced Materials, University of Groningen, Groningen 9747 AG, The Netherlands*

Li Qiu − *Zernike Institute for Advanced Materials and Stratingh Institute for Chemistry, University of Groningen, Groningen 9747 AG, The Netherlands*

Jan C. Hummelen − *Zernike Institute for Advanced Materials and Stratingh Institute for Chemistry, University of Groningen, Groningen 9747 AG, The Netherlands*

Giuseppe Portale − *Zernike Institute for Advanced Materials, University of Groningen, Groningen 9747 AG, The Netherlands;* orcid.org/0000-0002-4903-3159

Michael C. Heiber − *Center for Hierarchical Materials Design, Northwestern University, Evanston, Illinois 60208, United States*

Complete contact information is available at: https://pubs.acs.org/10.1021/acsami.0c15490

Author Contributions

‖M.K. and M.A.T.L. contributed equally to this work.

Notes

The authors declare no competing financial interest.

■ ACKNOWLEDGMENTS

The authors thank the Center for Information Technology of the University of Groningen for their support and for providing access to the Peregrine high-performance computing cluster. This work is part of the research program of the Foundation for Fundamental Research on Matter (FOM), which is part of the Netherlands Organization for Scientific Research (NWO). This is a publication by the FOM Focus Group "Next Generation Organic Photovoltaics", participating in the Dutch Institute for Fundamental Energy Research (DIFFER). This work was supported by a grant from STW/NWO (VIDI 13476). M.C.H. was supported by financial assistance award no. 70NANB14H012 from the U.S. Department of Com-

merce, National Institute of Standards and Technology, as part of the Center for Hierarchical Materials Design (CHiMaD).

REFERENCES

(1) Lüssem, B.; Riede, M.; Leo, K. Doping of Organic Semiconductors. *Phys. Status Solidi A* **2013**, *210*, 9−43.
(2) Salzmann, I.; Heimel, G. Toward a Comprehensive Understanding of Molecular Doping Organic Semiconductors (Review). *J. Electron Spectrosc. Relat. Phenom.* **2015**, *204*, 208−222.
(3) Le Corre, V. M.; Stolterfoht, M.; Perdigón Toro, L.; Feuerstein, M.; Wolff, C.; Gil-Escrig, L.; Bolink, H. J.; Neher, D.; Koster, L. J. A. Charge Transport Layers Limiting the Efficiency of Perovskite Solar Cells: How to Optimize Conductivity, Doping, and Thickness. *ACS Appl. Energy Mater.* **2019**, *2*, 6280−6287.
(4) Rowe, D. M. *Thermoelectrics Handbook*; Taylor & Francis: Boca Raton, 2006; p 1008.
(5) Salzmann, I.; Heimel, G.; Oehzelt, M.; Winkler, S.; Koch, N. Molecular Electrical Doping of Organic Semiconductors: Fundamental Mechanisms and Emerging Dopant Design Rules. *Acc. Chem. Res.* **2016**, *49*, 370−378.
(6) Aubry, T. J.; Axtell, J. C.; Basile, V. M.; Winchell, K. J.; Lindemuth, J. R.; Porter, T. M.; Liu, J. Y.; Alexandrova, A. N.; Kubiak, C. P.; Tolbert, S. H.; Spokoyny, A. M.; Schwartz, B. J. Dodecaborane-Based Dopants Designed to Shield Anion Electrostatics Lead to Increased Carrier Mobility in a Doped Conjugated Polymer. *Adv. Mater.* **2019**, *31*, No. 1805647.
(7) Bao, Q.; Liu, X.; Braun, S.; Gao, F.; Fahlman, M. Energetics at Doped Conjugated Polymer/Electrode Interfaces. *Adv. Mater. Interfaces* **2015**, *2*, No. 1400403.
(8) Deschler, F.; Riedel, D.; Deák, A.; Ecker, B.; Von Hauff, E.; Da Como, E. Imaging of Morphological Changes and Phase Segregation in Doped Polymeric Semiconductors. *Synth. Met.* **2015**, *199*, 381−387.
(9) Duong, D. T.; Wang, C.; Antono, E.; Toney, M. F.; Salleo, A. The Chemical and Structural Origin of Efficient P-Type Doping in P3HT. *Org. Electron.* **2013**, *14*, 1330−1336.
(10) Euvrard, J.; Revaux, A.; Bayle, P. A.; Bardet, M.; Vuillaume, D.; Kahn, A. The Formation of Polymer-Dopant Aggregates as a Possible Origin of Limited Doping Efficiency at High Dopant Concentration. *Org. Electron.* **2018**, *53*, 135−140.
(11) Harada, K.; Sumino, M.; Adachi, C.; Tanaka, S.; Miyazaki, K. Improved Thermoelectric Performance of Organic Thin-Film Elements Utilizing a Bilayer Structure of Pentacene and 2,3,5,6-Tetrafluoro-7,7,8,8-Tetracyanoquinodimethane (F4 -TCNQ). *Appl. Phys. Lett.* **2010**, *96*, No. 253304.
(12) Huang, D.; Yao, H.; Cui, Y.; Zou, Y.; Zhang, F.; Wang, C.; Shen, H.; Jin, W.; Zhu, J.; Diao, Y.; Xu, W.; Di, C. A.; Zhu, D. Conjugated-Backbone Effect of Organic Small Molecules for n-Type Thermoelectric Materials with ZT over 0.2. *J. Am. Chem. Soc.* **2017**, *139*, 13013−13023.
(13) Hwang, S.; Potscavage, W. J.; Yang, Y. S.; Park, I. S.; Matsushima, T.; Adachi, C. Solution-Processed Organic Thermoelectric Materials Exhibiting Doping-Concentration-Dependent Polarity. *Phys. Chem. Chem. Phys.* **2016**, *18*, 29199−29207.
(14) Kiefer, D.; Giovannitti, A.; Sun, H.; Biskup, T.; Hofmann, A.; Koopmans, M.; Cendra, C.; Weber, S.; Koster, L. J. A.; Olsson, E.; Rivnay, J.; Fabiano, S.; McCulloch, I.; Müller, C. Enhanced n-Doping Efficiency of a Naphthalenediimide-Based Copolymer through Polar Side Chains for Organic Thermoelectrics. *ACS Energy Lett.* **2018**, *3*, 278−285.
(15) Li, C. Z.; Chueh, C. C.; Yip, H. L.; Ding, F.; Li, X.; Jen, A. K. Y. Solution-Processible Highly Conducting Fullerenes. *Adv. Mater.* **2013**, *25*, 2457−2461.
(16) Li, C. Z.; Chueh, C. C.; Ding, F.; Yip, H. L.; Liang, P. W.; Li, X.; Jen, A. K. Doping of Fullerenes via Anion-Induced Electron Transfer and its Implication for Surfactant Facilitated High Performance Polymer Solar Cells. *Adv. Mater.* **2013**, *25*, 4425−4430.
(17) Li, J.; Rochester, C. W.; Jacobs, I. E.; Aasen, E. W.; Friedrich, S.; Stroeve, P.; Moulé, A. J. The Effect of Thermal Annealing on Dopant Site Choice in Conjugated Polymers. *Org. Electron.* **2016**, *33*, 23−31.
(18) Liu, J.; Qiu, L.; Portale, G.; Koopmans, M.; ten Brink, G.; Hummelen, J. C.; Koster, L. J. A. N-Type Organic Thermoelectrics: Improved Power Factor by Tailoring Host−Dopant Miscibility. *Adv. Mater.* **2017**, *29*, No. 1701641.
(19) Liu, J.; Qiu, L.; Portale, G.; Torabi, S.; Stuart, M. C. A.; Qiu, X.; Koopmans, M.; Chiechi, R. C.; Hummelen, J. C.; Koster, L. J. A. Side-Chain Effects on N-Type Organic Thermoelectrics: A Case Study of Fullerene Derivatives. *Nano Energy* **2018**, *52*, 183−191.
(20) Méndez, H.; Heimel, G.; Winkler, S.; Frisch, J.; Opitz, A.; Sauer, K.; Wegner, B.; Oehzelt, M.; Röthel, C.; Duhm, S.; Többens, D.; Koch, N.; Salzmann, I. Charge-Transfer Crystallites as Molecular Electrical Dopants. *Nat. Commun.* **2015**, *6*, No. 8560.
(21) Menke, T.; Ray, D.; Meiss, J.; Leo, K.; Riede, M. In-Situ Conductivity and Seebeck Measurements of Highly Efficient N-Dopants in Fullerene C60. *Appl. Phys. Lett.* **2012**, *100*, No. 093304.
(22) Paulsen, B. D.; Frisbie, C. D. Dependence of Conductivity on Charge Density and Electrochemical Potential in Polymer Semiconductors Gated with Ionic Liquids. *J. Phys. Chem. C* **2012**, *116*, 3132−3141.
(23) Méndez, H.; Heimel, G.; Opitz, A.; Sauer, K.; Barkowski, P.; Oehzelt, M.; Soeda, J.; Okamoto, T.; Takeya, J.; Arlin, J.-B.; Balandier, J.-Y.; Geerts, Y.; Koch, N.; Salzmann, I. Doping of Organic Semiconductors: Impact of Dopant Strength and Electronic Coupling. *Angew. Chem., Int. Ed.* **2013**, *52*, 7751−7755.
(24) Schlitz, R. A.; Brunetti, F. G.; Glaudell, A. M.; Miller, P. L.; Brady, M. A.; Takacs, C. J.; Hawker, C. J.; Chabinyc, M. L. Solubility-Limited Extrinsic N-Type Doping of a High Electron Mobility Polymer for Thermoelectric Applications. *Adv. Mater.* **2014**, *26*, 2825−2830.
(25) Scholes, D. T.; Hawks, S. A.; Yee, P. Y.; Wu, H.; Lindemuth, J. R.; Tolbert, S. H.; Schwartz, B. J. Overcoming Film Quality Issues for Conjugated Polymers Doped with F4TCNQ by Solution Sequential Processing: Hall Effect, Structural, and Optical Measurements. *J. Phys. Chem. Lett.* **2015**, *6*, 4786−4793.
(26) Liu, J.; Ye, G.; van der Zee, B.; Dong, J.; Qiu, X.; Liu, Y.; Portale, G.; Chiechi, R. C.; Koster, L. J. A. N-Type Organic Thermoelectrics of Donor−Acceptor Copolymers: Improved Power Factor by Molecular Tailoring of the Density of States. *Adv. Mater.* **2018**, *30*, No. 1804290.
(27) Liu, J.; van der Zee, B.; Alessandri, R.; Sami, S.; Dong, J.; Nugraha, M. I.; Barker, A. J.; Rousseva, S.; Qiu, L.; Qiu, X.; Klasen, N.; Chiechi, R. C.; Baran, D.; Caironi, M.; Anthopoulos, T. D.; Portale, G.; Havenith, R. W. A.; Marrink, S. J.; Hummelen, J. C.; Koster, L. J. A. The Phonon-Glass Electron-Crystal Concept in n-Type Organic Thermoelectrics: Demonstration of ZT > 0.3. *Nat. Commun.* **2020**, *11*, 5694.
(28) Liu, J.; Shi, Y.; Dong, J.; Nugraha, M. I.; Qiu, X.; Su, M.; Chiechi, R. C.; Baran, D.; Portale, G.; Guo, X.; Koster, L. J. A. Overcoming Coulomb Interaction Improves Free-Charge Generation and Thermoelectric Properties for n-Doped Conjugated Polymers. *ACS Energy Lett.* **2019**, *4*, 1556−1564.
(29) Kiefer, D.; Kroon, R.; Hofmann, A. I.; Sun, H.; Liu, X.; Giovannitti, A.; Stegerer, D.; Cano, A.; Hynynen, J.; Yu, L.; Zhang, Y.; Nai, D.; Harrelson, T. F.; Sommer, M.; Moulé, A. J.; Kemerink, M.; Marder, S. R.; McCulloch, I.; Fahlman, M.; Fabiano, S.; Müller, C. Double Dping of Conjugated Polymers with Monomer Molecular Dopants. *Nat. Mater.* **2019**, *18*, 149−155.
(30) Bässler, H. Charge Transport in Disordered Organic Photoconductors a Monte Carlo Simulation Study. *Phys. Status Solidi B* **1993**, *175*, 15−56.
(31) Arkhipov, V. I.; Heremans, P.; Emelianova, E. V.; Adriaenssens, G. J.; Bässler, H. Weak-Field Carrier Hopping in Disordered Organic Semiconductors: The Effects of Deep Traps and Partly Filled Density-of-States Distribution. *J. Phys.: Condens. Matter* **2002**, *14*, 9899−9911.
(32) Vissenberg, M. C. J. M.; Matters, M. Theory of the Field-Effect Mobility in Amorphous Organic Transistors. *Phys. Rev. B* **1998**, *57*, 12964−12967.

https://dx.doi.org/10.1021/acsami.0c15490
ACS Appl. Mater. Interfaces 2020, 12, 56222−56230

(33) Tanase, C.; Meijer, E. J.; Blom, P. W. M.; de Leeuw, D. M. Unification of the Hole Transport in Polymeric Field-Effect Transistorsand Light-Emitting Diodes. *Phys. Rev. Lett.* **2003**, *91*, No. 216601.
(34) Pasveer, W. F.; Cottaar, J.; Tanase, C.; Coehoorn, R.; Bobbert, P. A.; Blom, P. W. M.; de Leeuw, D. M.; Michels, M. A. J. Unified Description of Charge-Carrier Mobilities in Disordered Semiconducting Polymers. *Phys. Rev. Lett.* **2005**, *94*, No. 206601.
(35) Zuo, G.; Abdalla, H.; Kemerink, M. Impact of Doping on the Density of States and the Mobility in Organic Semiconductors. *Phys. Rev. B* **2016**, *93*, No. 235203.
(36) Mityashin, A.; Olivier, Y.; Van Regemorter, T.; Rolin, C.; Verlaak, S.; Martinelli, N. G.; Beljonne, D.; Cornil, J.; Genoe, J.; Heremans, P. Unraveling the Mechanism of Molecular Doping in Organic Semiconductors. *Adv. Mater.* **2012**, *24*, 1535−1539.
(37) Tietze, M. L.; Benduhn, J.; Pahner, P.; Nell, B.; Schwarze, M.; Kleemann, H.; Krammer, M.; Zojer, K.; Vandewal, K.; Leo, K. Elementary Steps in Electrical Doping of Organic Semiconductors. *Nat. Commun.* **2018**, *9*, No. 1182.
(38) Arkhipov, V. I.; Emelianova, E. V.; Heremans, P.; Bässler, H. Analytic Model of Carrier Mobility in Doped Disordered Organic Semiconductors. *Phys. Rev. B* **2005**, *72*, No. 235202.
(39) Arkhipov, V. I.; Heremans, P.; Emelianova, E. V.; Bässler, H. Effect of Doping on the Density-of-States Distribution and Carrier Hopping in Disordered Organic Semiconductors. *Phys. Rev. B* **2005**, *71*, No. 045214.
(40) Schwarze, M.; Gaul, C.; Scholz, R.; Bussolotti, F.; Hofacker, A.; Schellhammer, K. S.; Nell, B.; Naab, B. D.; Bao, Z.; Spoltore, D.; Vandewal, K.; Widmer, J.; Kera, S.; Ueno, N.; Ortmann, F.; Leo, K. Molecular Parameters Responsible for Thermally Activated Transport in Doped Organic Semiconductors. *Nat. Mater.* **2019**, *18*, 242−248.
(41) Abate, A.; Staff, D. R.; Hollman, D. J.; Snaith, H. J.; Walker, A. B. Influence of Ionizing Dopants on Charge Transport in Organic Semiconductors. *Phys. Chem. Chem. Phys.* **2014**, *16*, 1132−1138.
(42) Liu, F.; van Eersel, H.; Xu, B.; Wilbers, J. G. E.; de Jong, M. P.; van der Wiel, W. G.; Bobbert, P. A.; Coehoorn, R. Effect of Coulomb Correlation on Charge Transport in Disordered Organic Semiconductors. *Phys. Rev. B* **2017**, *96*, No. 205203.
(43) Efros, A. L.; Shklovskii, B. I. Coulomb Gap and Low Temperature Conductivity of Disordered Systems. *J. Phys. C: Solid State Phys.* **1975**, *8*, L49.
(44) Efros, A. L. Coulomb Gap in Disordered Systems. *J. Phys. C: Solid State Phys.* **1976**, *9*, 2021−2030.
(45) Shi, K.; Zhang, F.; Di, C. A.; Yan, T. W.; Zou, Y.; Zhou, X.; Zhu, D.; Wang, J. Y.; Pei, J. Toward High Performance n-Type Thermoelectric Materials by Rational Modification of BDPPV Backbones. *J. Am. Chem. Soc.* **2015**, *137*, 6979−6982.
(46) Tal, O.; Rosenwaks, Y.; Preezant, Y.; Tessler, N.; Chan, C. K.; Kahn, A. Direct Determination of the Hole Density of States in Undoped and Doped Amorphous OrganicFilms with High Lateral Resolution. *Phys. Rev. Lett.* **2005**, *95*, No. 256405.
(47) Shen, Y.; Diest, K.; Wong, M. H.; Hsieh, B. R.; Dunlap, D. H.; Malliaras, G. G. Charge Transport in Doped Organic Semiconductors. *Phys. Rev. B* **2003**, *68*, No. 081204.
(48) Shklovskii, B. I.; Efros, A. L. *Electronic Properties of Doped Semiconductors*, 1st ed.; Springer-Verlag: Berlin Heidelberg, 1984; pp 60−237.
(49) Barth, S.; Bässler, H. Intrinsic Photoconduction in PPV-Type Conjugated Polymers. *Phys. Rev. Lett.* **1997**, *79*, 4445−4448.
(50) Jahani, F.; Torabi, S.; Chiechi, R. C.; Koster, L. J. A.; Hummelen, J. C. Fullerene Derivatives with Increased Dielectric Constants. *Chem. Commun.* **2014**, *50*, 10645−10647.
(51) Miller, A.; Abrahams, E. Impurity Conduction at Low Concentrations. *Phys. Rev.* **1960**, *120*, 745−755.
(52) Heiber, M. C. Excimontec v1.0: An Open-Source Software Tool for Kinetic Monte Carlo Simulations of Organic Electronic Devices. *J. Open Source Software* **2020**, *5*, No. 2307.
(53) Heiber, M. C.; Nguyen, T. Q.; Deibel, C. Charge Carrier Concentration Dependence of Encounter-Limited Bimolecular Recombination in Phase-Separated Organic Semiconductor Blends. *Phys. Rev. B* **2016**, *93*, No. 205204.

https://dx.doi.org/10.1021/acsami.0c15490
ACS Appl. Mater. Interfaces 2020, 12, 56222−56230